Adsorption of nucleotides on clay surfaces: Effects of mineral composition, pH and solution salts

Pierre Mignon, Gwenaëlle Corbin, Sébastien Le Crom, Virginie Marry, Jihua Hao, Isabelle Daniel

Adsorption of Nucleotides on Clay Surfaces. Effects of mineral composition, pH and solution salts.

Pierre Mignon[1], Gwenaëlle Corbin[1], Sébastien Le Crom[2], Virginie Marry[2], Jihua Hao[3,4], Isabelle Daniel[3]

[1] Institut Lumière Matière, UMR 5306, Université Claude Bernard Lyon 1, CNRS, Université de Lyon, 69622 Villeurbanne cedex, France ; [2] Laboratoire PHENIX, Sorbonne Université/CNRS UMR 8234, case 51, 4 Place Jussieu, F-75005 Paris, France ; [3] Univ Lyon, Université Lyon 1, ENS de Lyon, CNRS, UMR 5276 LGL-TPE, F-69622 Villeurbanne, France; [4] Department of Marine and Coastal Sciences, Rutgers University, 71 Dudley RD, New Brunswick, NJ-08901, USA

Abstract:

In the context of the origin of life, the adsorption of nucleotides onto clay surfaces has been tackled through classical molecular dynamics calculations. The effect of the mineral composition, pH and solution salts has been explored. It was firstly observed that cation adopts a layered structure above mineral surfaces which changes as a function of mineral composition and surface charge location, and has substantial effects on nucleotide adsorption. If the mineral charge is located in the octahedral (inner) layer of montmorillonite, the first two layers are less populated while the third comprises the majority of cations. For nontronite, which presents negative charges in the tetrahedral layer in contact with solutes, the first two layers concentrate the majority of cations. The negative charge on clay surface is thus screened by the first two layers for nontronite, and the third layer for montmorillonite. As a result, negatively charged phosphate moiety of nucleotides, which coordinates cations, can approach closer to the surface and the nucleobase binds better to the surface of nontronite compared to montmorillonite. As such, the nucleobase interacts in a parallel configuration stabilized by Van der Waals interactions with the surface. This observation explains the experimental results on the effect of mineral composition as well as pH and aqueous cations. Indeed, at pH=3, the nucleobase and phosphate protonation states lead to a different adsorption mode, where phosphate does not play any role whilst the positively charged nucleobase does participate actively in binding to the clay surface through electrostatic interactions. In presence of divalent cations in solution, the phosphate does coordinate exclusively to the divalent cations. Ca^{2+} cation exchange in the second layer allows the coordinated phosphate to approach closer to the surface and leads to nucleobase adsorption in a parallel configuration.

Introduction.

In the prebiotic context that requires to form complex biomolecules, the role of clay minerals is still a matter of debate. As a result of aqueous or hydrothermal alteration of the seafloor iron magnesium rich silicates, clay minerals were already abundant on Earth during late Hadean or early Archean periods when life originated (Hazen et al., 2013; Pearce et al., 2018). These clays have been recognized to offer multiple interesting properties for the potential concentration and polymerization of the building blocks of biomolecules present in the first living organisms. The primitive seawater was probably very dilute in organics (Miller, 1987), primitive atmosphere had no ozone layer, therefore minerals would play the role of geochemical niches allowing for accumulation of biomolecules' precursors and protect them from UV radiation. In particular clays, as layered and charged materials, offer a large surface and a reactive environment which may have facilitated the organics' or biomolecules' synthesis, adsorption, and polymerization (Hazen and Sverjensky, 2010; Cleaves et al., 2012; Lambert et al., 2012; Rimola et al., 2013).

Adsorption of biomolecules and in particular nucleotides onto clays' surface has been extensively studied via experimental and theoretical approaches. For example, thirty years ago, Ferris investigated the adsorption of nucleotides onto (Al-Mg)-rich swelling clay montmorillonite (Ferris, 1989, 1993, 2005), followed by a series of works with activated nucleotides, which showed that clay surface could catalyze the polymerization leading to RNA oligomers as long as 50-mers (Ferris, 2002). Recently, experimental studies investigated the adsorption of non-activated nucleotides onto clays under various environmental conditions, including mineral composition, pH, and salinity. The results showed that 5'-monophosphate deoxyribose and 5'-monophosphate ribose nucleotides behave in a similar way on the surface of Fe-Mg-rich and Al-rich phyllosilicates, independent of the nucleobase (Feuillie et al., 2013). Under conditions analogous to modern seawater, i.e. 0.5 M NaCl and 0.05 M $MgCl_2$, and nearly neutral pH, a ligand exchange mechanism has been proposed with the phosphate group of the nucleotides binding the metal-hydroxyl groups of the edge surfaces of phyllosilicates (Pedreira-Segade et al., 2016). However, this adsorption mode tends to preclude further polymerization since a free phosphate group is mandatory to the formation of the phosphodiester bond that makes the backbone of oligonucleotides. The effect of various salts has been considered with swelling and non-swelling phyllosilicates (Pedreira-Segade et al., 2018). It was proposed that divalent cations (Mg^{2+} or Ca^{2+}) would preferably lead to cationic bridging adsorption on basal surfaces, *i.e.* through cation coordination by the negatively charged phosphate group. Interestingly, this mechanism indicates a higher retention capacity of the swelling clays compared to non-swelling phyllosilicates (Pedreira-Segade et al., 2018a). In agreement with the cation bridging mode by the phosphate group, combined experimental and computational approaches have shown that 5'AMP binds better onto montmorillonite as compared to

adenine and adenosine at high salts concentration solutions (Villafañe-Barajas et al., 2018). The effect of high concentrations of transition metal cations, potentially representative of the primitive ocean, on nucleotides adsorption has also been studied recently (Hao et al., 2018). It was observed that transition metal salts led to an increase of the adsorption up to twice or more for Zn^{2+} as compared to Na^{+}. Moreover, clay composition and solution pH seem to have important influences on the adsorption, for all considered salts. Indeed, nontronite, a Fe-rich clay which carries negative charges in the surface tetrahedral layer (Al substituted SiO_2 layer), displays a better nucleotide retention on its surface as compared to montmorillonite (Mg-rich), which carries negative charges in the sandwiched octahedral layer (Mg substituted AlO_3 layer). A higher adsorption is observed at acidic pH=3 than at pH=7 for alkali and earth-alkali cations.

In the present study we aim at assessing the possible adsorption modes and molecular interactions responsible for the retention of nucleotides on clays' surface through classical molecular dynamics (MD) simulations. Various theoretical studies have addressed the interaction of biomolecules with mineral surfaces in order to describe and understand adsorption modes and reactivity (Rimola et al., 2013, 2019). In particular the study of adsorption of nucleobases on montmorillonite surface, via both static and dynamic DFT calculations, highlighted the possible physisorption modes (Mignon et al., 2009; Mignon and Sodupe, 2012, 2013). It suggested that nucleobases may bind through H-bonding perpendicular to the surface or through dispersion/Van der Waals interactions parallel to the surface. The interaction significantly increases when the nucleobase coordinates a cation, corresponding to the cation bridging adsorption mode. Potential adsorption through H-bonding was also possible at the hydroxylated edge clay surfaces (Mignon et al., 2019). In comparison with DFT calculations, classical MD simulations permit to considerably increase size and time scale of the system. Well parametrized force fields allow, with a reasonable accuracy, exploring more adsorption modes and assessing the affinity of the nucleobase for the mineral surface in conditions close to experimental ones. Only very few MD studies have been devoted to the adsorption of nucleotides on clay surfaces. Stacking interaction of adenine nucleobase on the surface was observed in a MD simulation of nucleotides in montmorillonite interlayer (Mathew and Luthey-Schulten, 2010). In the presence of Ca^{2+}, cation-phosphate coordination was observed, and it was argued that oligonucleotide may adsorb in the interlayer. This definitely requires further investigation since the primitive seawater composition may have been largely different from present-day : higher Ca, lower Mg, high Fe(II) and Mn(II) (Halevy and Bachan, 2017; Krissansen-Totton et al., 2018; Marty et al., 2018; Tosca et al., 2019), thus allowing interlayer cation exchange and the presence of divalent cations at the basal surface of clays. More recently MD simulations have highlighted other adsorption modes of nucleotides (Pedreira-Segade et al., 2018a) with a possibly preferential adsorption of GMP on the basal surface of montmorillonite in

presence of Ca^{2+} cations in solution. It was observed that the phosphate may coordinate to cations and the nucleobase interacts with the mineral surface directly through H-bonding or Van der Waals interactions. Following these investigations, we tackle in the present study the effect of environmental conditions on the adsorption of nucleotides by varying the pH, clay composition and salts in solution through classical MD modelling. The deoxyguanosine monophosphate (dGMP) nucleotide is considered as a model like in recent experiments (Hao et al., 2018; Pedreira-Segade et al., 2018b). Its different protonation states according to considered pKas are considered in order to mimic acidic and neutral pH. Nontronite and montmorillonite are the clay minerals investigated here; their difference in compositions allows to understand the role of surface charges on nucleotide adsorption. Finally, the effect of monovalent vs. divalent cations is assessed *via* Na^+ or Ca^{2+} containing models.

Computational Details.

Models. Clay models have been built from the X-Ray data of pyrophyllite (Lee and Guggenheim, 1981), which has been refined through DFT calculations. Unit-cell dimension and atoms positions were optimized using the PBE functional through periodic plane waves calculations with the VASP package (Kresse and Hafner, 1993; Kresse and Furthmüller, 1996). Optimized cell parameters were very close to experimental ones (less than 2% variation): a=5.083Å, b=8.897Å, c=9.410Å, α=90.12°, β=100.58°, γ= 89.94°. Since only one layer is considered in our model, the cell was changed to orthorhombic. In order to model the basal surface, the basic box was built by multiplying a x 6 and b x 4 leading to box basal dimensions: a=30.498Å and b=35.588Å. Clay composition was set according to previous experimental works (Feuillie et al., 2013; Hao et al., 2018). Montmorillonite composition: $(Si_{7.95}\ Al_{0.05}\ )(Al_{2.75}\ Fe^{3+}_{0.17}\ Mg_{1.07})O_{20}\ (OH)_4\ Na_{1.11}$ was modelled through 26 octahedral substitutions Al^{3+} by Mg^{2+}; Nontronite composition $(Si_{6.98}\ Al_{0.95}\ Fe^{3+}_{0.07}\ )(Al_{0.36}\ Fe_{3.61}\ Mg_{0.04})O_{20}\ (OH)_4\ Na_{1.05}$ was approximated by including 24 Si^{4+} by Al^{3+} tetrahedral substitutions and 86 Al^{3+} by Fe^{3+} octahedral substitutions; the latter not leading to any layer charges. Atomic substitutions were done randomly respecting the rule separation between octahedral substitutions: at least one octahedral center between two substitutions. Na^+ counter-cations were included in solution according to the number of substitutions in the mineral layer. Na^+-Cl^- pairs were added to the water molecules initially added to the system, in agreement with the experimental conditions of 0.5 M NaCl aqueous solutions (Hao et al., 2018).

The nucleotide geometries and charge parameters were refined through DFT calculation at the B3LYP/6-31G* level. Nucleotides were optimized in the gas phase and then RESP atomic partial charges reproducing the electrostatic potential on a molecular surface have been used (Woods and Chappelle, 2000). Two protonated states were considered for dGMP according to guanine's and phosphate's pKas (Shabarova and Bogdanov, 1994) and the selected pH value of the simulations (Figure 1). At acidic pH

close to pH=3, the phosphate group carries one negative charge while almost 50% of the aqueous guanine moiety is positively charged. At pH<3, guanine is protonated at N7 and the phosphate group carries one negative charge, referred as $dG^{+}mP^{-}$. At pH=7 guanine is neutral and the phosphate group carries two negative charges, it will be referred as $dGmP^{2-}$. Figure 1 shows the geometries of the nucleotides.

The ClayFF force field was used for clay models (Cygan et al., 2004) while water and ions were modelled using the SPC/E and Dang models, respectively (Berendsen et al., 1981; Dang, 1995). The SPC/E model is known to accurately reproduce water structure. The General Amber Force Field (Wang et al., 2004) was used to generate nucleotide parameters and Lorentz-Berthelot rules were applied for inter force fields parameters. This approach has already been successfully used in various theoretical works (Thyveetil et al., 2008; Swadling et al., 2010, 2012, 2013). The Amber force field has been extensively used in nucleic acids modelling and reproduces well the structure and dynamics of nucleic acid moeites (Cheatham III and Young, 2000; Thyveetil et al., 2008; Swadling et al., 2010). Amber and ClayFF are rather simple to combine since both use harmonic potential for bond terms, although ClayFF uses neither angle nor dihedral terms. Periodic boundary conditions were applied in all three spatial directions.

The large-scale atomistic/molecular massively parallel simulator (LAMMPS) (Plimpton, 1995) was used for all simulations. A unique clay layer was considered to model the basal surface, and it was divided half at the bottom and top of the box along the *z* vertical parameter. The initial separation was set to 60 Å, the nucleotide was placed in the center of the box, water molecules filled the empty space in a regular grip (with a 3.3 Å interval) including the amount of Na^{2+}, Ca^{2+} and Cl^{-} needed to get a total neutral charge. A cutoff of 12 Å was applied to the electrostatic and Lennard-Jones interactions. Coulombic interactions were computed by Ewald summation and the particle-particle, particle-mesh method at a 0.0001 accuracy. All simulations were carried out at 300 K and 1 atm. The oxygen-hydrogen bonds of water molecules were maintained fixed by applying the shake algorithm (Ryckaert et al., 1977). The equilibration period consisted in warming up the system, starting from water/ions moiety then the clays particles and the nucleotide, successively, via the NVT ensemble. The system was then allowed to relax along all directions through the NPT ensemble. This step allowed to fix the vertical separation between basal surfaces for the whole production. The system was then equilibrating through two steps increasing the time step from 0.1 to 0.5 fs. The whole equilibration spent 800000 time steps. During the whole simulation and production, the octahedral atoms were maintained fixed. The production time during which data were analyzed was 100 ns for all simulations.

Results and Discussion.

In order to study the effects of mineral composition, pH and aqueous cations, simulations were performed through the same equilibration/production procedures for all systems. Mineral composition has been tackled by considering the montmorillonite and nontronite minerals; pH effect was studied with $dGMP^{2-}$ and $dG^{+}MP^{-}$ nucleotides at pH=7 and pH=3, respectively; and mono-/di-valent cations effects were investigated by adding 0.05M $CaCl_2$ salt to the initial 0.5M NaCl solution.

Mineral composition effect. Density profiles along the z coordination are shown in Figure 2 for $dGMP^{2-}$ and $dG^{+}MP^{-}$ nucleotides and both montmorillonite and nontronite minerals. The first and most distinctive property for both minerals is the Na^{+} cation density near clay surfaces. One notices a cationic structure made of three layers. For montmorillonite, the first peak is at 0.55 - 0.85 Å, the second at 2.55-2.75 Å, and the third one at 4.10-4.20 Å, representing 6.7-6.8 %, 7.4-11.1 % and 35.0-37.2 % of the total amount of aqueous cations in the system, respectively (data given for $dGMP^{2-}$ and $dG^{+}MP^{-}$ nucleotides in Table 1). For nontronite, the values of peaks' positions and cations amount (in parentheses) are: 0.50-0.55 Å (19.0-19.3 %), 2.00-2.05 Å (32.2-32.4 %) and 4.20-4.25 Å (10.9-12.7 %). This shows that the first two peaks are closer to the surface of nontronite as compared to montmorillonite; the difference is striking for the second peak. The first two layers are also much more populated for nontronite, which contains 51.4-51.5 % of all aqueous cations, as compared to montmorillonite, whose cation density remains as low as 14.1-17.9 %. The total cation density near the surface is higher for nontronite than for montmorillonite: 62.4-64.1 % and 51.3-52.9 %, respectively. This difference is clearly due to the distribution of negative charges, which are located on the surface oxygen atoms of nontronite because of tetrahedral substitution as opposed to montmorillonite which negative charges are located on the internal oxygen atoms due to octahedral substitutions. The effects of this charge distribution are quite striking as almost the whole negative charge of the nontronite platelet is screened by cation; only 0.3 to 0.9 of the total 24.0 negative charges on the surface are not screened by Na^{+} cations. For montmorillonite, 5.1 to 6.0 negative charges are not screened over the 26.0 total negative charges. As a result, the negative charge is much less visible on nontronite surface from the bulk solution because of a much denser cation population in the first two layers above surface. It's also noticeable that the minimum density between the second and third cation layers for nontronite is well marked, showing a clear distinction between the third and the first two layers.

At pH=7, *i.e.* for $dGMP^{2-}$, the phosphate group of the nucleotide is found to be located at around 3.95 Å above the surface oxygen atoms of nontronite for more than 61% of the simulation and at 6.90 Å for the remaining time. In addition, the O6 atom of guanine is located close to the nontronite surface at 3.05 Å for more than 81% of the simulation. In comparison, the phosphate group remains further away from the montmorillonite surface at about 6.60-6.65 Å from the bottom and the top surfaces for 25.2%

and 60.2% of the simulation, respectively, representing 85.4% of the simulation. The nucleobase position related to phosphate's position is present at 3.25 Å from the montmorillonite surface during 4.4 % of the simulation. According to the radial distribution function (rdf) between the P atom of the phosphate and Na^+ cations, the negatively charged phosphate coordinates almost two cations during the simulation on montmorillonite (N=1.84) and nontronite (N=1.83) (see Table 2 for coordination numbers and first peak maximum obtained from radial distribution analysis). The sodium cation is around 2.35 Å away from phosphate oxygen atoms. This result suggests a strong affinity of the $-HPO_4^{2-}$ group for cations and thus strong phosphate-cation coordination may explain the different behavior in nucleotide adsorption. Indeed, because of the layer structure of cations above clays' surface, the phosphate approaches the surface where most cations are located and screen the negative charge of the surface, thus alleviating electrostatic repulsion between clay's negative surface and the phosphate. For montmorillonite, the third cation layer at around 4.15 Å above the surface is the most populated. In this case, the phosphate tends to coordinate the cations of this layer, because the first two layers do not screen the negative charge of the surface due to low cation density. As such, the phosphate group remains at a distance of about 6.60 Å, which does not allow the nucleobase to approach close to the surface. At pH=7 guanine remains far from the surface of montmorillonite during most of the simulation at 6.15 - 8.45 Å (see Table 1) or interact through H-bonding as shown in Figure 3a, only 4.4% of the simulation. The results is different for nontronite, which negative surface charge is almost totally screened, and the first two cation layers are the most populated, thus responsible for most of charge screening. As a result, the phosphate approaches the cation layer and penetrates deeper to 3.95 Å from the surface (Table 1) and coordinate cations of the second layer that is the densest layer (Figure 3b). The fact that the phosphate can approach close to nontronite's surface may allow the nucleobase to adsorb closely onto the surface, *i.e.* at 3.05 Å. At such a short distance from the nontronite's surface the nucleobase is engaged in planar adsorption mode with the surface to maximize Van der Waals interactions for more than 80% of the simulation (Figure 3b). Such an interaction between the nucleobase and the surface has already been observed in previous calculations, which showed that the base is stabilized through both Van der Waals interactions and cation coordination with O6 guanine atom (Mignon et al., 2009; Mignon and Sodupe, 2013). Although the coordination number is only 0.32, the guanine coordinated Na^+ cation is at a distance of 2.44 Å, thus showing a rather strong coordination.

pH effect. By comparing density profiles with dG^+MP^- and $dGMP^{2-}$ corresponding to pH=3 (Figure 2a & 2b) and pH=7 (Figure 2c & 2d), respectively, we can evaluate the effect of the pH on nucleotide adsorption onto montmorillonite or nontronite. The most important difference between dG^+MP^- and $dGMP^{2-}$ arises from the adsorption of the nucleobase. Indeed, for montmorillonite, guanine remains

adsorbed on the surface for 33.4 % of the simulation at pH=3 whilst it is limited to 3.4 % at pH=7. For nontronite the difference is less pronounced; the nucleobase is adsorbed on the surface during the whole simulation at pH=3 and somehow less (81.2 %) at pH=7. The Na^+ coordination by O6 is also less important for dG^+MP^-; the coordination number is less than 0.2 with a larger O6-Na^+ distance between 2.46 and 2.48 Å, as compared to p=7 (see Table 2 for coordination numbers and first peak maximum obtained from radial distribution analysis). Finally, and most importantly, the coordination of the phosphate toward Na^+ is almost negligible at pH=3, coordination numbers and first peak maximum distances are 0.04/3.16 Å and 0.14/3.63 Å for montmorillonite and nontronite, respectively, as compared to 1.84/3.04 Å and 1.83/3.06 Å at pH=7. This shows that the nucleotide adsorption at pH=3 is obviously not due to the electrostatic interaction between the phosphate and Na^+ cations organized in layers above the surface; at pH=3 the phosphate group carries only one negative charge. At pH=3 nucleotide adsorption is due the attraction of the positively charged guanine nucleobase by the negative surface charges, leading to a very strong adsorption onto the clay surface (Figure 4). In contrast adsorption pH=7 is due to phosphate interactions with Na^+ surface layers allowing for the nucleobase to approach the surface being stabilized through Van der Waals interactions.

Salts effects. The effect of divalent cations has been tackled by adding Ca^{2+} cation in solution at two concentrations, at pH=7 and evaluating the effect on the adsorption onto nontronite surface. The first low concentration of 0.05 M $CaCl_2$ is equivalent to that used experimentally (Hao et al., 2018), and corresponds to 2 additional Ca^{2+} cations in the simulation box. The effect of the added Ca^{2+} cations was not clearly visible during the time given for the simulation; 2 Ca^{2+} among 37 Na^+ do not allow to observe any change in the layers above clay surface. The second concentration is equivalent to a 0.25 M $CaCl_2$ solution, is higher than that used by Hao et al. (2018) and allows to observe the effect of Ca^{2+} cations in our model. This concentration corresponds to 7 additional $CaCl_2$ in the simulation box, and the only Na^+ cations present are counter cations due to substitutions' charge compensation. Such a high concentration is still relevant for the early seawater (Halevy and Bachan, 2017; Krissansen-Totton et al., 2018). Firstly, we observe that one Ca^{2+} cation is almost always coordinated to the phosphate group, showing the very high affinity of Ca^{2+} for the -PO_4^{2-} group. Coordination numbers and distances (computed from the P-Ca radial distribution function, Table 2) are 0.88/2.87 Å and 0.98/2.93 Å for low and high Ca^{2+} concentration, respectively. One may notice the low coordination numbers and large distances between Na^+ and P (computed from P-Na^+ rdf), 0.26/3.60 Å at high Ca^{2+} concentration. This shows that Na^+ cation is absent in the first phosphate coordination sphere when a Ca^{2+} is coordinated to the nucleotide phosphate moiety. Thus in presence of a divalent cation, the coordination of phosphate with cations is almost exclusive.

Density profiles for both systems are shown in Figure 5. For the low Ca^{2+} concentration system, only a few configurations have been sampled when Ca^{2+} cations have been found in the 2nd cation layer, and half a Ca^{2+} cation is found in the third layer, statistically over the simulation. As a result, the phosphate group remains rather far from the surface mainly at 5.15 and 5.85 Å (Table 3). However, this does not prevent the guanine from strongly binding the surface; it adsorbs the surface at 3.05 Å for 85 % of the simulation in a parallel configuration as shown in Figure 7a. For the high concentration system, 1-2 Ca^{2+} and 0.6-1.2 Ca^{2+} can be found in the second and third cation layers above the surface, respectively. As above-mentioned, the high Ca^{2+} concentration allowed to sample more the 2nd layer Ca^{2+} cation exchange configurations, in agreement with experiments over a longer time scale. The 2nd layer cation exchange by divalent cation, mainly coordinated to the phosphate group allows the phosphate to approach closer to the surface as shown by a high density (50.1 %) of the phosphate group at 3.30 Å only of the surface (Table 3). This distance corresponds to the shortest distance between the phosphate and the surface among all the simulations run in the present study. As a result, one can see that the nucleotide density is almost entirely (91.2 %) located at 3.15 Å, which corresponds to a planar adsorption of the nucleotide of the surface, thus maximizing the Van der Waals interaction (Figure 7b).

Conclusion.

The classical MD simulations carried out in this study allowed us to investigate the effect of mineral composition, pH, salinity, and salt concentration on nucleotide adsorption onto clay surfaces. Mineral composition has substantial effects on nucleotide adsorption.

First, we observed that cations close to the negatively charged surface are structured in three layers above the surface at about 0.5-0.8 Å, 2.0-2.7 Å and 4.1-4.2 Å, respectively. The layers' density may change as function of mineral composition and charge location on their basal surface. If the charge is located in the octahedral (inner)clay layer, the two first cations layers are less populated while the third layer comprises most cations. If the negative charge is located in the tetrahedral layer just in contact with solutes, the first two cations layers concentrates the majority of the aqueous cations. As a result, the negative surface charge is screened and the negatively charged nucleotide phosphate group can coordinate cations preferentially in the most populated cation layer. This screening allows the nucleobase to bind the surface in a coplanar configuration, maximizing Van der Waals interactions. Secondly, at acidic pH protonated species due to the protonation of guanine N7 site at pH=3 for instance, may bind the negatively charged clay surface through electrostatic (and Van der Waals still present) interactions. Moreover, in that case the adsorption is completely driven by this interaction; no phosphate-cation coordination was observed at this low pH. This again shows the importance of the negative surface charge towards adsorption. Finally, the effect of the aqueous divalent cations is

found to be preponderant since the -PO_4^{2-} group does coordinate exclusively these divalent cations. As a result, due to cation exchange and the presence of these cations in the layers' structure above the surface, the phosphate group approaches very close to the mineral surface through strong cation coordination and allows nucleobase binding. The effect of cations is predominant toward nucleotide adsorption while it may be tuned by varying mineral composition and pH; the effect of the latter potentially involving a different adsorption mode, driven by different molecular interactions.

Acknowledgments.

P.M., G.C. and I.D. gratefully acknowledge financial support from the Défi/CNRS 'Origines 2018'. Calculations were performed using HPC resources from GENCI- [IDRIS] (Grant A0030807662- [gen7662]). This work is also financially supported by The French National Research Agency through the PREBIOM (Primitive Earth - Biomolecules Interacting with Hydrothermal Oceanic Minerals) project #ANR-15-CE31-0010. J. H. acknowledges the postdoctoral fellowship from LABEX Lyon Institute of Origins (ANR-10-LABX-0066) of the Université de Lyon within the program "Investissements d'Avenir" (ANR-11-IDEX-0007) of the French government operated by the National Research Agency (ANR).

Table 1. Density profiles data corresponding to Figure 2. Peaks' distances from top or bottom surface oxygen atoms are given in Å and their integral are given in percentage of the number of the considered atoms (Na^+, O6, P) present in the simulation box

			Os - Na^+			Os - O6	Os - P
			1rst layer	2nd layer	3rd layer		
pH = 3	Montmorillonite	Top surface	0.85 (2.7)	2.55 (4.1)	4.20 (20.2)	-	-
		Bottom surface	0.55 (4.0)	2.60 (3.3)	4.10 (17.0)	2.95 (33.4) - 5.60 (18.5)	6.90 (24.8) - 10.35 (35.3)
	Nontronite	Top surface	0.50 (8.9)	2.05 (18.5)	4.20 (6.0)	3.15 (49.5)	6.65 (54.3)
		Bottom surface	0.50 (10.4)	2.00 (13.7)	4.20 (4.9)	3.15 (41.5)	6.55 (41.3)
pH = 7	Montmorillonite	Top surface	0.80 (3.2)	3.75 (7.7)	4.20 (17.9)	3.25 (4.4) - 6.15 (10.3) - 8.45 (14.0)	6.65 (60.2)
		Bottom surface	0.55 (3.6)	2.55 (3.4)	4.15 (17.1)	-	6.60 (25.2)
	Nontronite	Top surface	0.50 (8.6)	2.05 (17.6)	4.20 (5.8)	-	-
		Bottom surface	0.55 (10.4)	2.05 (14.8)	4.25 (6.9)	3.05 (81.2) - 10.25 (10.9)	3.95 (61.2) - 6.9 (26.9)

Table 2. Coordination data obtained from radial distribution function analysis. First peak maximum distances given in Å.

Salt	nucleotide	Clay	P-Na		O6-Na		P-Ca		O6-Ca	
			Coord. Nb	dist.	Coord. Nb	dist.	Coord. Nb	dist.	Coord. Nb	dist.
NaCl	$dG^{+}mP^{-}$	MNT	0,04	3,16	0,20	2,46				
		NNT	0,14	3,63	0,17	2,48				
	$dGmp^{2-}$	MNT	1,84	3,04	0,35	2,44				
		NNT	1,83	3,06	0,32	2,44				
$NaCl + CaCl_2$ [0,05 M]	$dGmp^{2-}$	NNT	0,48	2,38	0,37	2,43	0,88	2,87	0,02	2,40
$CaCl_2$ [0,25 M]		NNT	0,23	3,60	0,19	2,42	0,98	2,93	0,01	2,43

Table 3. Density profiles data corresponding to Figure 4. Peaks' distances from top or bottom surface oxygen atoms are given in Å and their integral are given in percentage of the number of the considered atoms (Na^+, O6, P) present in the simulation box

		Os - Ca^{2+}			Os - O6	Os - P
		1rst layer	2nd layer	3rd layer		
NaCl [0.5] + $CaCl_2$ [0.05]	Top surface	-	-	4.30 (1.8)	-	-
	Bottom surface	-	2.20 (14.9)	4.25 (27.8)	5.05 (85.8)	5.15 (32.9) - 5.85 (57.3)
$CaCl_2$ [0.25]	Top surface	-	2.05 (28.7)	4.25 (8.8)	-	-
	Bottom surface	-	2.15 (13.7)	4.25 (17.2)	3.15 (91.2)	3.30 (50.1) - (5.70 (16.6) - 6.05 (25.3)

Figure 1. Protonation states of dGmP as a function of pH and pKas (Shabarova and Bogdanov, 1994).

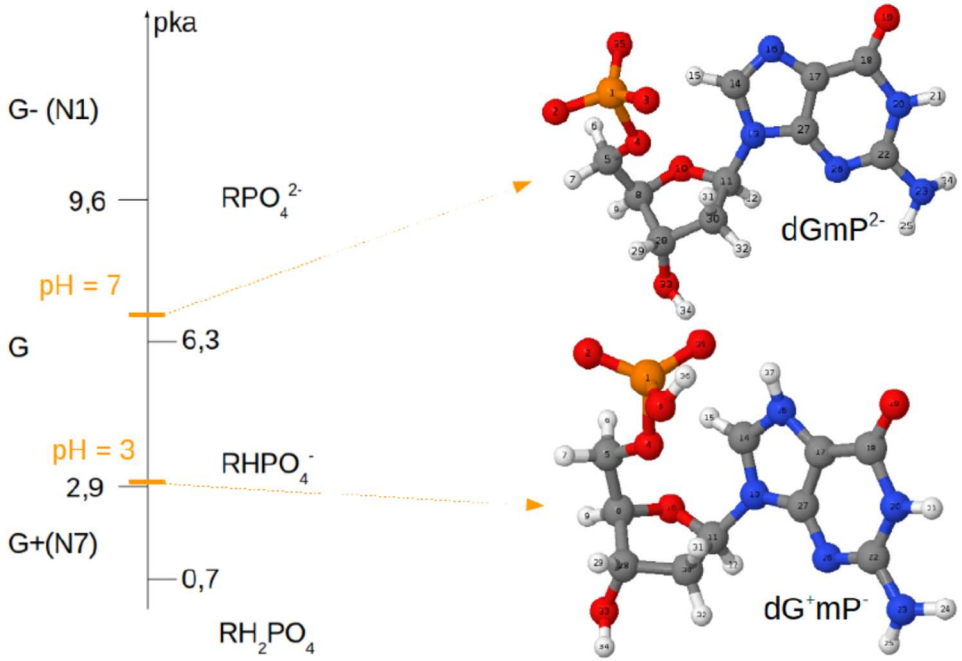

Figure 2. Density profiles along z coordinate for a) $dG^{+}mP^{-}$ with montmorillonite, b) $dG^{+}mP^{-}$ with nontronite, c) $dGmP^{2-}$ with montmorillonite, d)$dGmP^{2-}$ with nontronite Surface oxygen atoms Os are depicted in black, water oxygens in blue, Na^{+} cations in pink, O6 of guanine and P of the phosphate group of the nucleotide in red and orange respectively.

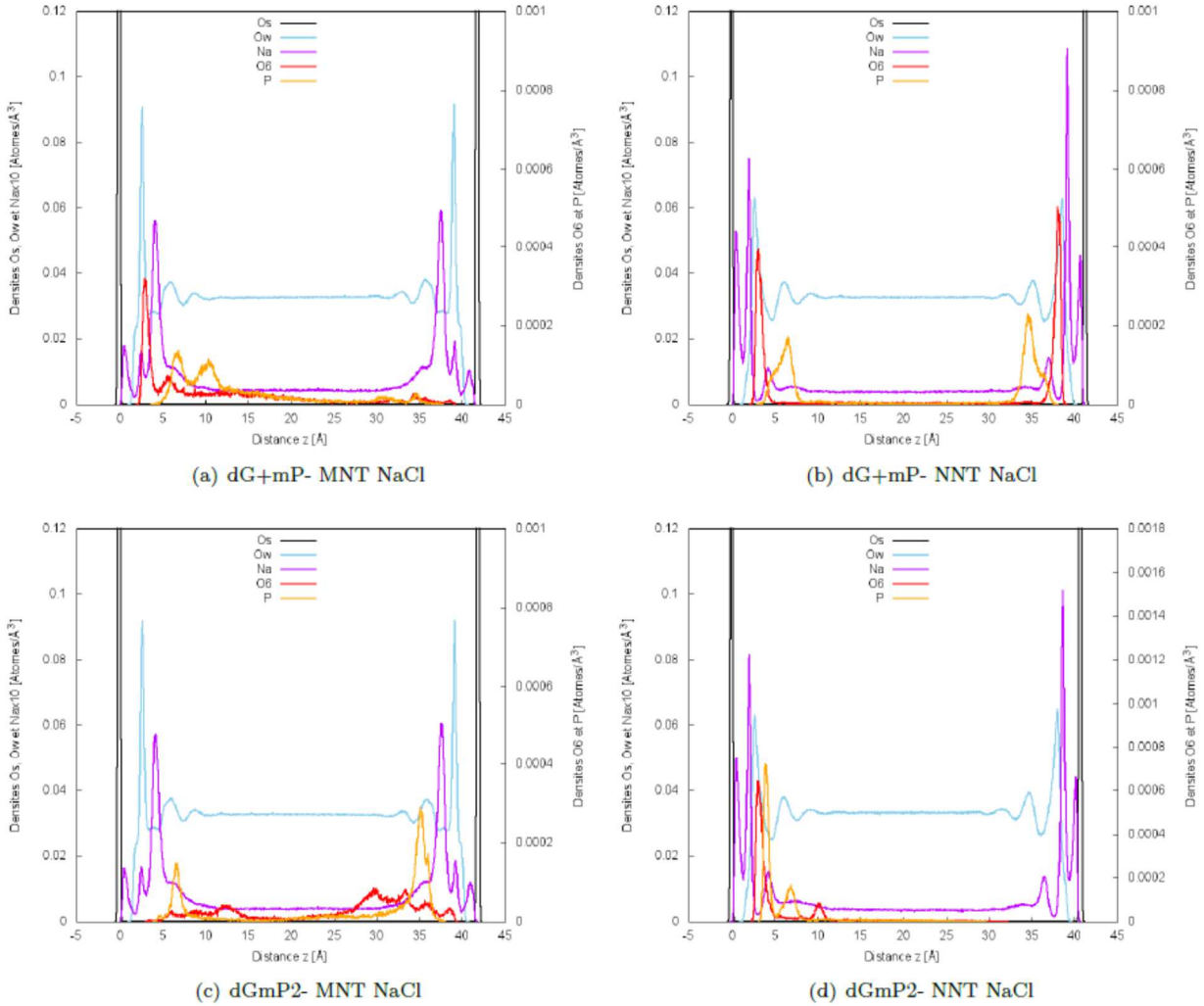

(a) dG+mP- MNT NaCl

(b) dG+mP- NNT NaCl

(c) dGmP2- MNT NaCl

(d) dGmP2- NNT NaCl

Figure 3. Snapshots of (a) $dGmp^{2-}$ adsorbed on montmorillonite surface, and (b) on nontronite surface. Distances are given in Å.

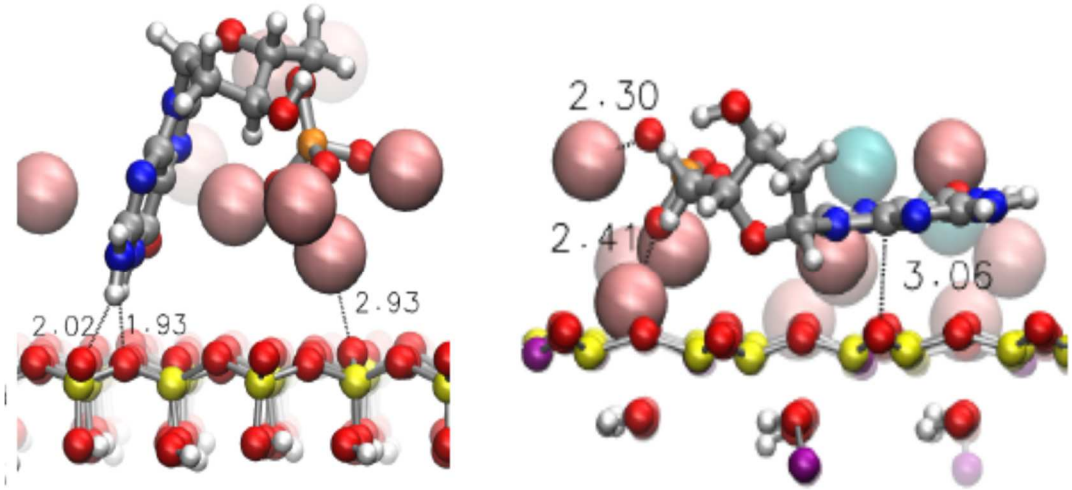

Figure 4. Snapshots of (a) $dG^{+}mp^{-}$ adsorbed on montmorillonite surface, and (b) on nontronite surface. Distances are given in Å.

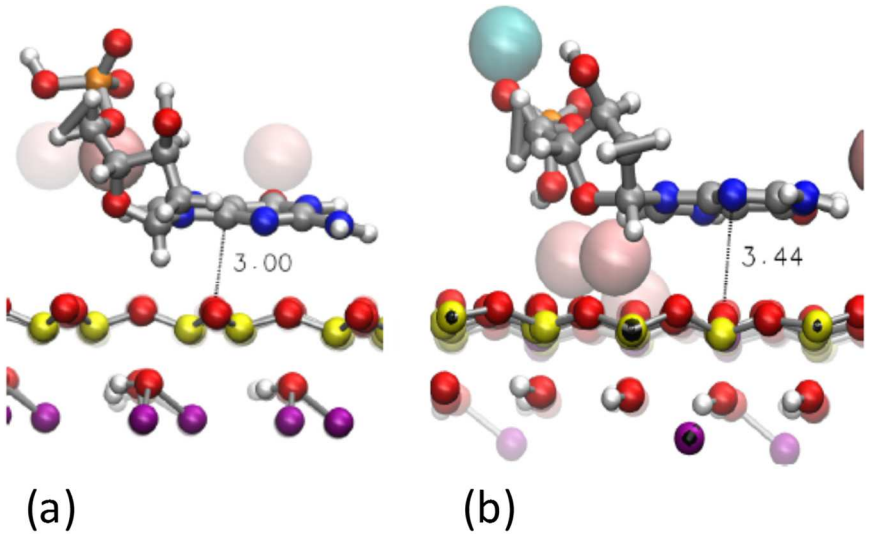

Figure 5. Density profiles along z coordinate for $dGmP^{2-}$ with nontronite at a) low [0.05M] $CaCl_2$ concentration, b) at high [0.25 M] $CaCl_2$ concentration. Surface oxygen atoms Os are depicted in black, water oxygens in blue, Na^+ cations in pink, Ca^{2+} in green, O6 of guanine and P of the phosphate group of the nucleotide in red and orange respectively.

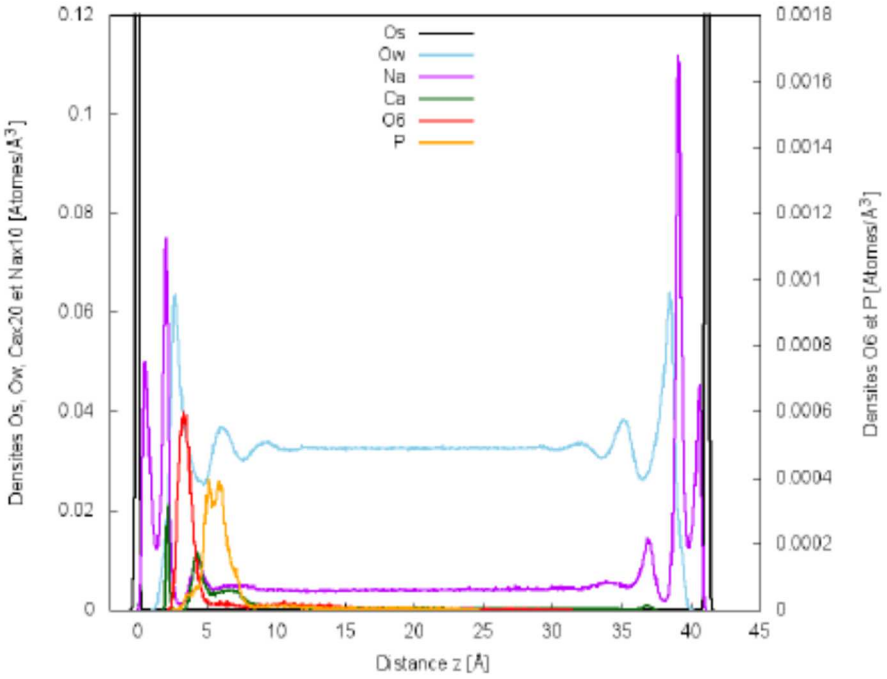

(a) dGmP2- NNT NaCl+$CaCl_2$

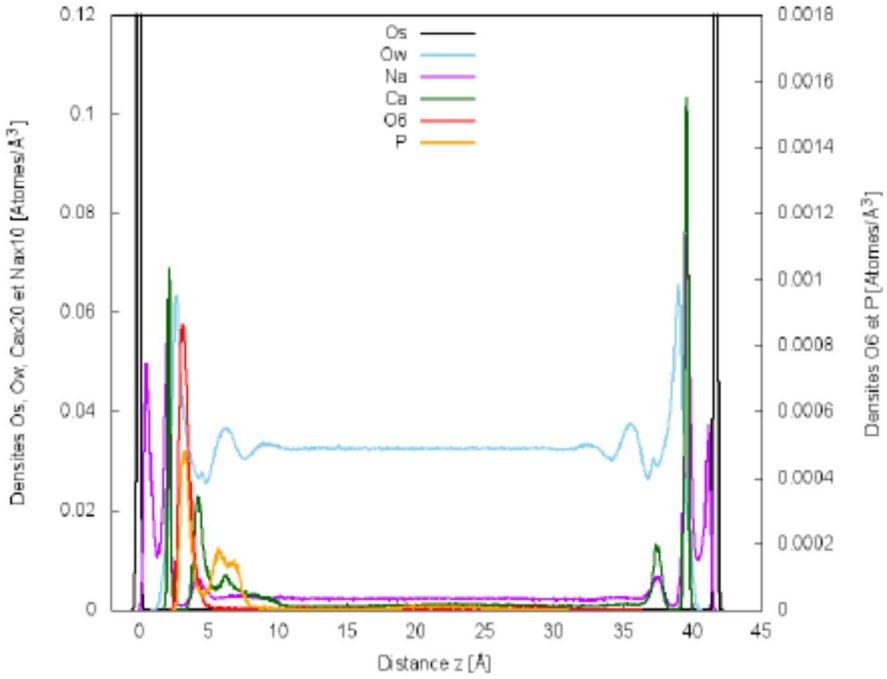

(b) dGmP2- NNT $CaCl_2$

Figure 7. Snapshots $dGmp^{2-}$ adsorbed on nontronite surface at (a) low and (b) high Ca^{2+} concentrations. Distances are given in Å.

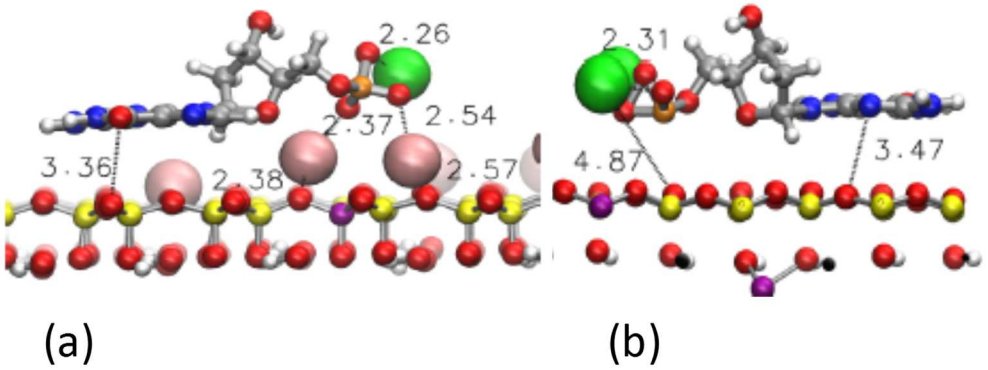

References

Berendsen, H.J.C., Postma, J.P.M., Van Gunsteren, W.F., Hermans, J., 1981. Interaction models for water in relation to protein hydration. Jerusalem Symp. Quantum Chem. Biochem. FIELD Full Journal Title:Jerusalem Symposia on Quantum Chemistry and Biochemistry 14, 331–42.

Cheatham III, T.E., Young, M.A., 2000. Molecular dynamics simulation of nucleic acids: Successes, limitations, and promise*. Biopolymers 56, 232–256. https://doi.org/10.1002/1097-0282(2000)56:4<232::AID-BIP10037>3.0.CO;2-H

Cleaves, H.J., Michalkova Scott, A., Hill, F.C., Leszczynski, J., Sahai, N., Hazen, R., 2012. Mineral-organic interfacial processes: potential roles in the origins of life. Chem. Soc. Rev. 41, 5502–5525.

Cygan, R.T., Liang, J.-J., Kalinichev, A.G., 2004. Molecular models of hydroxide, oxyhydroxide, and clay phases and the development of a general force field. J. Phys. Chem. B FIELD Full Journal Title:Journal of Physical Chemistry B 108, 1255–1266.

Dang, L.X., 1995. Mechanism and Thermodynamics of Ion Selectivity in Aqueous Solutions of 18-Crown-6 Ether: A Molecular Dynamics Study. J. Am. Chem. Soc. 117, 6954–6960. https://doi.org/10.1021/ja00131a018

Ferris, J.P., 2005. Mineral catalysis and prebiotic synthesis: Montmorillonite-catalyzed formation of RNA. Elements 1, 145–149.

Ferris, J.P., 2002. Montmorillonite catalysis of 30-50 mer oligonucleotides: Laboratory demonstration of potential steps in the origin of the RNA world. Origins of Life and Evolution of the Biosphere 32, 311–332.

Ferris, J.P., 1993. Montmorillonite Catalysis of Rna Oligomer Formation in Aqueous-Solution - a Model for the Prebiotic Formation of Rna. Journal of the American Chemical Society 115, 12270–12275.

Ferris, J.P., 1989. The Adsorption of Nucleotides and Polynucleotides on Montmorillonite Clay. Origins of Life and Evolution of the Biosphere 19, 153–164.

Feuillie, C., Daniel, I., Michot, L.J., Pedreira-Segade, U., 2013. Adsorption of nucleotides onto Fe–Mg–Al rich swelling clays. Geochimica et Cosmochimica Acta 120, 97–108. https://doi.org/10.1016/j.gca.2013.06.021

Halevy, I., Bachan, A., 2017. The geologic history of seawater pH. Science (Washington, DC, U. S.) 355, 1069–1071. https://doi.org/10.1126/science.aal4151

Hao, J., Mokhtari, M., Pedreira-Segade, U., Michot, L.J., Daniel, I., 2018. Transition Metals Enhance the Adsorption of Nucleotides onto Clays: Implications for the Origin of Life. ACS Earth and Space Chemistry. https://doi.org/10.1021/acsearthspacechem.8b00145

Hazen, R.M., Sverjensky, D.A., 2010. Mineral Surfaces, Geochemical Complexities, and the Origins of Life. Cold Spring Harbor Perspectives in Biology 2, a002162–a002162. https://doi.org/10.1101/cshperspect.a002162

Hazen, R.M., Sverjensky, D.A., Azzolini, D., Bish, D.L., Elmore, S.C., Hinnov, L., Milliken, R.E., 2013. Clay mineral evolution. American Mineralogist 98, 2007–2029. https://doi.org/10.2138/am.2013.4425

Kresse, G., Furthmüller, J., 1996. Efficient iterative schemes for ab initio total-energy calculations using a plane-wave basis set. Phys. Rev. B 54, 11169.

Kresse, G., Hafner, J., 1993. Ab initio molecular dynamics for open-shell transition metals. Physical Review B: Condensed Matter and Materials Physics 48, 13115–18.

Krissansen-Totton, J., Arney, G.N., Catling, D.C., 2018. Constraining the climate and ocean pH of the early Earth with a geological carbon cycle model. Proc. Natl. Acad. Sci. U. S. A. 115, 4105–4110. https://doi.org/10.1073/pnas.1721296115

Lambert, J.-F., Sodupe, M., Ugliengo, P., 2012. Prebiotic chemistry. Chemical Society Reviews 41, 5373. https://doi.org/10.1039/c2cs90061k

Lee, J.H., Guggenheim, S., 1981. Single crystal X-ray refinement of pyrophyllite-1Tc. American Mineralogist 66, 350–357.

Marty, B., Avice, G., Bekaert, D.V., Broadley, M.W., 2018. Salinity of the Archaean oceans from analysis of fluid inclusions in quartz. COMPTES RENDUS GEOSCIENCE 350, 154–163. https://doi.org/10.1016/j.crte.2017.12.002

Mathew, D.C., Luthey-Schulten, Z., 2010. Influence of Montmorillonite on Nucleotide Oligomerization Reactions: A Molecular Dynamics Study. Origins of Life and Evolution of Biospheres 40, 303–317. https://doi.org/10.1007/s11084-010-9207-0

Mignon, P., Navarro-Ruiz, J., Rimola, A., Sodupe, M., 2019. Nucleobase Stacking at Clay Edges, a Favorable Interaction for RNA/DNA Oligomerization. ACS Earth Space Chem. 3, 1023–1033. https://doi.org/10.1021/acsearthspacechem.9b00021

Mignon, P., Sodupe, M., 2013. Structural Behaviors of Cytosine into the Hydrated Interlayer of Na^+-Montmorillonite Clay. An ab Initio Molecular Dynamics Study. The Journal of Physical Chemistry C 117, 26179–26189. https://doi.org/10.1021/jp4103383

Mignon, P., Sodupe, M., 2012. Theoretical study of the adsorption of DNA bases on the acidic external surface of montmorillonite. Phys. Chem. Chem. Phys. 14, 945–954. https://doi.org/10.1039/c1cp22454a

Mignon, P., Ugliengo, P., Sodupe, M., 2009. Theoretical Study of the Adsorption of RNA/DNA Bases on the External Surfaces of Na+-Montmorillonite. Journal of Physical Chemistry C 113, 13741–13749.

Miller, S.L., 1987. Which Organic Compounds Could Have Occurred on the Prebiotic Earth? Cold Spring Harbor Symposia on Quantitative Biology 52, 17–27. https://doi.org/10.1101/SQB.1987.052.01.005

Pearce, B.K.D., Tupper, A.S., Pudritz, R.E., Higgs, P.G., 2018. Constraining the Time Interval for the Origin of Life on Earth. Astrobiology 18, 343–364. https://doi.org/10.1089/ast.2017.1674

Pedreira-Segade, U., Feuillie, C., Pelletier, M., Michot, L.J., Daniel, I., 2016. Adsorption of nucleotides onto ferromagnesian phyllosilicates: Significance for the origin of life. Geochimica et Cosmochimica Acta 176, 81–95. https://doi.org/10.1016/j.gca.2015.12.025

Pedreira-Segade, U., Hao, J., Razafitianamaharavo, A., Pelletier, M., Marry, V., Le Crom, S., Michot, L., Daniel, I., 2018a. How do Nucleotides Adsorb Onto Clays? Life 8, 59. https://doi.org/10.3390/life8040059

Pedreira-Segade, U., Michot, L.J., Daniel, I., 2018b. Effects of salinity on the adsorption of nucleotides onto phyllosilicates. Physical Chemistry Chemical Physics 20, 1938–1952. https://doi.org/10.1039/C7CP07004G

Plimpton, S., 1995. Fast Parallel Algorithms for Short-Range Molecular Dynamics. Journal of Computational Physics 117, 1–19. https://doi.org/10.1006/jcph.1995.1039

Rimola, A., Costa, D., Sodupe, M., Lambert, J.-F., Ugliengo, P., 2013. Silica Surface Features and Their Role in the Adsorption of Biomolecules: Computational Modeling and Experiments. Chem. Rev. 113, 4216–4313.

Rimola, A., Sodupe, M., Ugliengo, P., 2019. Role of Mineral Surfaces in Prebiotic Chemical Evolution. In Silico Quantum Mechanical Studies. Life 9, 10. https://doi.org/10.3390/life9010010

Ryckaert, J.-P., Ciccotti, G., Berendsen, H.J.C., 1977. Numerical integration of the cartesian equations of motion of a system with constraints: molecular dynamics of n-alkanes. Journal of Computational Physics 23, 327–341. https://doi.org/10.1016/0021-9991(77)90098-5

Shabarova, Z., Bogdanov, A., 1994. Advanced Organic Chemistry of Nucleic Acids, 1st ed. Wiley. https://doi.org/10.1002/9783527615933

Swadling, J.B., Coveney, P.V., Christopher Greenwell, H., 2012. Stability of free and mineral-protected nucleic acids: Implications for the RNA world. Geochim. Cosmochim. Acta 83, 360–378. https://doi.org/10.1016/j.gca.2011.12.023

Swadling, J.B., Coveney, P.V., Greenwell, H.C., 2010. Clay Minerals Mediate Folding and Regioselective Interactions of RNA: A Large-Scale Atomistic Simulation Study. Journal of the American Chemical Society 132, 13750–13764. https://doi.org/10.1021/ja104106y

Swadling, J.B., Suter, J.L., Greenwell, H.C., Coveney, P.V., 2013. Influence of Surface Chemistry and Charge on Mineral–RNA Interactions. Langmuir 29, 1573–1583. https://doi.org/10.1021/la303352g

Thyveetil, M.A., Coveney, P.V., Greenwell, H.C., Suter, J.L., 2008. Computer simulation study of the structural stability and materials properties of DNA-intercalated layered double hydroxides. J. Am. Chem. Soc. 130, 4742–4756.

Tosca, N.J., Jiang, C.Z., Rasmussen, B., Muhling, J., 2019. Products of the iron cycle on the early Earth. Free Radical Biology and Medicine 140, 138–153. https://doi.org/10.1016/j.freeradbiomed.2019.05.005

Villafañe-Barajas, S.A., Baú, J.P.T., Colín-García, M., Negrón-Mendoza, A., Heredia-Barbero, A., Pi-Puig, T., Zaia, D.A.M., 2018. Salinity Effects on the Adsorption of Nucleic Acid Compounds on Na-Montmorillonite: a Prebiotic Chemistry Experiment. Origins of Life and Evolution of Biospheres. https://doi.org/10.1007/s11084-018-9554-9

Wang, J., Wolf, R., Caldwell, J., Kollman, P., Case, D., 2004. Development and testing of a general amber force field. JOURNAL OF COMPUTATIONAL CHEMISTRY 25, 1157–1174. https://doi.org/10.1002/jcc.20035

Woods, R.J., Chappelle, R., 2000. Restrained electrostatic potential atomic partial charges for condensed-phase simulations of carbohydrates. Journal of Molecular Structure: THEOCHEM 527, 149–156. https://doi.org/10.1016/S0166-1280(00)00487-5